Remote Sensing Letters
Vol. 3, No. 7, 10 December 2012, 621–630

Taylor & Francis
Taylor & Francis Group

Land subsidence in the Nile Delta of Egypt observed by persistent scatterer interferometry

MOHAMED H. ALY*†, ANDREW G. KLEIN‡, HOWARD A. ZEBKER§ and JOHN R. GIARDINO‡

†Department of Earth Sciences, University of California-Riverside, Riverside, CA 92521, USA

‡Department of Geography, Texas A&M University, College Station, TX 77843, USA

§Department of Geophysics, Stanford University, Stanford, CA 94305, USA

(*Received 17 October 2011; in final form 17 December 2011*)

Land subsidence is a common problem in vulnerable deltas. The Nile Delta is no exception. The impacts of land subsidence are heightened by the economic, social and historical importance of the delta to Egypt. A major debate has evolved in the past two decades concerning whether the land surface of the Nile Delta is subsiding. The debate is certainly problematic in light of the fact that current measures of subsidence across the delta are rough estimates at best. To date, knowledge of subsidence rates in the delta is limited to long-term geologic averages that assume spatial uniformity and temporal consistency. In this study, we apply persistent scatterer interferometry (PSI) to measure the magnitude and monitor the spatial and temporal variations of land subsidence in the Nile Delta, during 1993–2000, using synthetic aperture radar interferometric data of 5.66 cm wavelength. The average measured rates of local subsidence in two major cities in the delta, namely Mansura and Greater Mahala, are –9 and –5 mm year^{-1}, respectively. The observed deformation features imply that subsidence in both cities is controlled mainly by local groundwater processes. Our PSI measurements indicate that no regional subsidence has occurred in either city between 1993 and 2000. The slight regional subsidence that is expected to occur over time due to the natural compaction of deltaic sediments most likely has been masked by surface displacements caused by seasonal oscillations in the groundwater level.

1. Introduction

Land subsidence is a global problem, particularly in vulnerable coastal areas such as the Nile Delta (figure 1(*a*)) and may induce major environmental problems. Potential consequences of land subsidence in the delta may include reduction in the capacity of the aquifer system, sinking of the coastal zone cities, and damaging of the utility infrastructures, railroads, highways and flyover bridges. Subsidence in the Nile Delta poses a need for regular monitoring and accurate measuring of its rates and patterns to help the decision-makers make informed decisions regarding the integrated development of the delta and the sustainable use of its natural resources.

*Corresponding author. Email: dr.m.aly@gmail.com

Remote Sensing Letters
ISSN 2150-704X print/ISSN 2150-7058 online © 2012 Taylor & Francis
http://www.tandf.co.uk/journals
http://dx.doi.org/10.1080/01431161.2011.652311

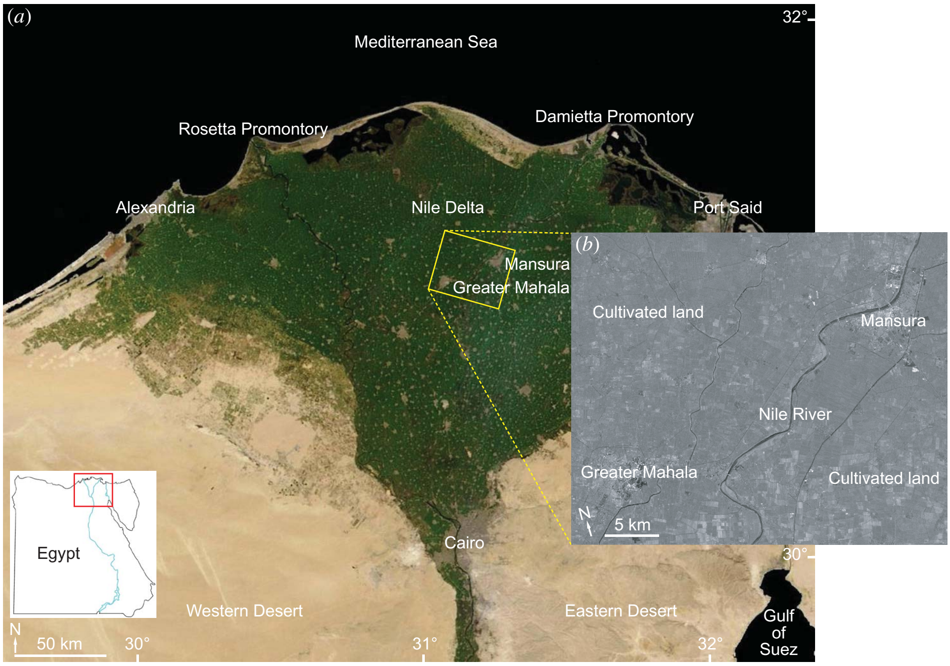

Figure 1. (*a*) The Nile Delta of Egypt as seen by the Moderate Resolution Imaging Spectroradiometer (MODIS) on 5 February 2003. The footprint of the ERS sub-scene (Track: 436, Frame: 2979) is shown with solid yellow lines. (*b*) The average amplitude image of 37 ERS sub-scenes spanning 1993–2000; dark grey tones indicate low amplitudes and bright tones indicate high amplitudes. Mansura and Greater Mahala appear in bright grey tones while the Nile River, irrigation channels and major roads appear in dark grey tones. Some crop fields appear in light grey tones.

Several factors contribute to the rates and patterns of subsidence across the delta. The main factors include tectonic activity, natural sediment compaction and hydrocarbon extraction, as well as groundwater pumping. During the past century, the rate of groundwater pumping in the delta increased extensively due to the dramatic change in the population density. According to the World Bank report (1990), the population of Egypt has increased from 10 million in 1890 to 65 million in 1990, with an average rate of increase of about 1 million people per year. The approximate population of Egypt is currently 80 million; about 50 million of them inhabit the Nile Delta. Groundwater-induced subsidence is thus expected in all metropolitan areas across the delta because the stratigraphic sequence of the delta consists mainly of clays, silts and sands.

Previous geologic studies indicate that the Nile Delta is presently subsiding. Stanley (1990) studied the Holocene deltaic sediments in the northern zone of the delta and radiocarbon-dated many of them. His study revealed differential long-term subsidence near the Mediterranean coast with average rates of 1.0–2.5 mm year^{-1} in the west and 5.0 mm year^{-1} in the east. Zaghloul *et al*. (1977), Stanley (1988, 1990) and Stanley and Warne (1993) attributed the rapid rate of subsidence in the eastern side of the delta to stratigraphic and tectonic factors. Zaghloul *et al*. (1990) studied the geomorphologic and geologic evolution, as well as subsidence, in the delta and reported similar rates of long-term subsidence during the Quaternary. Warne and Stanley (1993) studied several archaeological sites along the delta margin to reassess and refine the previously reported rates of subsidence. Their study concluded that subsidence rates estimated by Stanley (1990) in the northern part of the delta are minimum rates because radiocarbon-dated core ages are generally older than the ages of final burial as a result of sediment reworking.

To date, the actual rates of subsidence and their spatial and temporal variations across the delta are not well known because all measures from previous geologic studies are rough estimates at best. In contrast, synthetic aperture radar interferometry (InSAR) can provide subtle measurements of surface movements at a considerably improved spatial resolution with millimetre-level accuracy over large areas, approximately 100 km × 100 km for the European Remote-Sensing Satellites (ERS-1 and ERS-2). Numerous researchers (e.g. Galloway *et al*. 1998, Ferretti *et al*. 2000, Hoffmann *et al*. 2001, Buckley *et al*. 2003, Casu *et al*. 2005, Dixon *et al*. 2006, Aly *et al*. 2009, Osmanoğlu *et al*. 2011) successfully applied various InSAR techniques to study land subsidence.

With about 5 mm year^{-1} subsidence rate in the Nile Delta, approximately 1.12 rad year^{-1} of phase change in the slant range is expected in the topographically corrected interferograms generated from ERS images. Considering this slow rate of surface movements and phase ambiguity problems related to temporal and geometrical decorrelations in the densely vegetated delta, as well as anticipated strong tropospheric effects, it is difficult to obtain reliable measurements of subsidence in the delta using conventional InSAR techniques. In this study, we apply persistent scatterer interferometry (PSI) to overcome the traditional problems associated with conventional InSAR and to precisely monitor the spatial and temporal variations of subsidence in two major cities in the Nile Delta, namely Mansura and Greater Mahala (figure 1(*a*) and 1(*b*)), between 1993 and 2000. Interferometric measurements over these two cities, as well as over other cities, can provide a broad understanding of the subsidence phenomenon and its associated potential hazards in the vulnerable Nile Delta.

2. ERS data set and PSI analysis

Thirty-nine descending ERS scenes acquired over 8 years (1993–2000) are used in the PSI analysis. Details of the ERS scenes are provided in table 1. A small subset about 34 km × 24 km (figure 1(*b*)) of the 39 ERS images covering the study sites is processed to produce single look complex (SLC) images. Then, the SLC images are re-sampled and precisely registered to the ERS-2 scene acquired on 11 January 1996, which minimizes the temporal and perpendicular baselines in the ERS data set. Multi-looked amplitude images are created by taking 10 looks in the azimuth direction and 2 looks in the range direction to reduce the speckle and produce images with homogenous 40-m pixel dimensions. Detailed steps of the PSI approach we have conducted in this study are provided in our previous paper (Aly *et al*. 2009). Below we brief the key procedure we have followed to precisely measure subsidence in the study sites and create a time series of displacement maps.

Before selecting the persistent scatterers (PSs), all ERS images are calibrated radiometrically to make them comparable. The amplitude images are then averaged and the mean of the stack and the standard deviation from the mean are calculated. The average calibration factor for each image in the stack is calculated using the ratio of the amplitude of each image to the mean amplitude of the entire stack. PSs are identified

Table 1. ERS scenes used in the PSI analysis for Mansura and Greater Mahala.

Date	Perpendicular baseline, $B_{\perp}$ (m)	Temporal baseline, B_{T} (days)	ERS satellite
1 February 1993	−698.4072	−1074	1
12 April 1993	613.3302	−1004	1
17 May 1993	−94.7692	−969	1
26 July 1993	231.6942	−899	1
30 August 1993	−400.5836	−864	1
4 October 1993	−51.6256	−829	1
8 November 1993	165.0499	−794	1
20 July 1995	42.9351	−175	2
23 August 1995	−27.9726	−141	1
24 August 1995	−126.1882	−140	2
27 September 1995	139.3528	−106	1
28 September 1995	549.8912	−105	2
11 January 1996	0.0000	0	2
14 February 1996	638.1264	34	1
15 February 1996	648.0047	35	2
29 May 1996	−357.2229	139	1
30 May 1996	−463.6777	140	2
15 May 1997	24.4539	490	2
17 September 1998	−764.5666	980	2
31 December 1998	−782.0326	1085	2
11 March 1999	−77.6046	1155	2
15 April 1999	726.9202	1190	2
20 May 1999	−188.5021	1225	2
7 October 1999	−309.1264	1365	2
11 November 1999	318.2996	1400	2
16 December 1999	531.7678	1435	2
20 January 2000	−131.4232	1470	2
23 February 2000	−891.4721	1504	2
24 February 2000	−725.9152	1505	2
30 March 2000	−297.6116	1540	1
4 May 2000	−217.8680	1575	2
8 June 2000	−158.1932	1610	2
13 July 2000	−985.9117	1645	2
17 August 2000	−35.7963	1680	2
21 September 2000	690.2563	1715	2
26 October 2000	−305.6683	1750	2
30 November 2000	−223.2472	1785	2

using the amplitude dispersion index, which is used as a measure of phase stability. Points of low-amplitude dispersion, $d_{\mathrm{a}} < 0.25$, are selected as PSs with an average density of 64 and 51 PS km^{-2} in Mansura and Greater Mahala, respectively, using the following relation:

$$d_{\mathrm{a}} = \frac{\sigma_{\mathrm{a}}}{\mu_{\mathrm{a}}}, \tag{1}$$

where d_{a} is the amplitude dispersion index, σ_{a} is the standard deviation of the amplitude and μ_{a} is the mean of the amplitude.

There are no PSs identified in the densely vegetated areas because of the seasonal cultivation, flood irrigation and crop growth. The vegetation cover in the delta is basically seasonal crops that are changing dynamically every 4 months. Even the density of PSs identified in the urban areas is relatively low because of the constructional activities in both cities that lead to local interferometric phase decorrelation.

The complex interferograms are constructed from the SLC values extracted for the selected PSs by multiplying the reference image with the complex conjugate of the re-sampled images. All interferograms are found generally noisy. The location of the two cities in the centre of the densely vegetated delta, in addition to their limited spatial extents, make the local troposphere over the urban areas be saturated by the water vapour. As a preliminary assessment of the atmospheric artefacts in our ERS data set, interferograms of high correlation created from pairs of very short temporal baselines are compared using the pairwise comparison approach developed by Massonnet and Feigl (1995). The comparison reveals that winter acquisitions are generally less impacted by atmospheric effects than summer acquisitions. Two images acquired in summer 1998 are found plagued by atmospheric artefacts and thus are excluded from further analysis.

Digital elevation data of 3 arcseconds acquired by the Shuttle Radar Topographic Mission (SRTM) are used to correct the interferometric phase for topography. Then the non-linear adaptive filter developed by Goldstein and Werner (1998) is applied to reduce the phase noise in the topographically corrected interferograms. The precise state vectors determined by the Delft Institute for Earth-Oriented Space research (Scharoo and Visser 1998) are used to compensate for orbital inaccuracies. Subsequently, the corrected interferograms are integrated in time to produce a time series of unwrapped phase values for the selected PSs.

The created interferograms are inspected again and corrected for potential phase errors. As no measurable surface movements are expected to occur in the study area within a few days, phase signals observed in the topographically corrected interferograms of very short temporal baselines are considered atmospheric effects and/or topographic residuals and thus are filtered out. According to Zebker *et al.* (1997), phase signals that lack consistency in space and time are also considered atmospheric artefacts rather than real deformation and are filtered out. The effect of soil moisture and topographically induced artefacts are not considered a source of error because our PSs are selected in urban areas only and the study sites have flat terrains. The line-of-sight (LOS) surface displacement maps are created eventually from the iteratively corrected interferograms.

3. Results and discussion

Thirty-seven LOS surface displacement maps, covering the time period 1993–2000 and referenced temporally to the initially selected reference (ERS-2 image acquired on 11 January 1996), are created for Mansura and Greater Mahala. The average measured rates of surface displacements away from the satellite in the LOS direction are –9 and –5 mm year^{-1}, respectively. The mean LOS displacements superimposed on the average amplitude images are shown in figure 2(*a*) and 2(*c*).

Three PSs (PSa, PSb and PSc) are selected in each city to demonstrate the behaviour of deformation during 1993–2000. Locations of the selected PSs are shown in figure 2(*a*) and 2(*c*) and their deformation phase histories are presented in figure 2(*b*) and 2(*d*). In Mansura, the deformation phase history of PSa (figure 2(*b*)) demonstrates

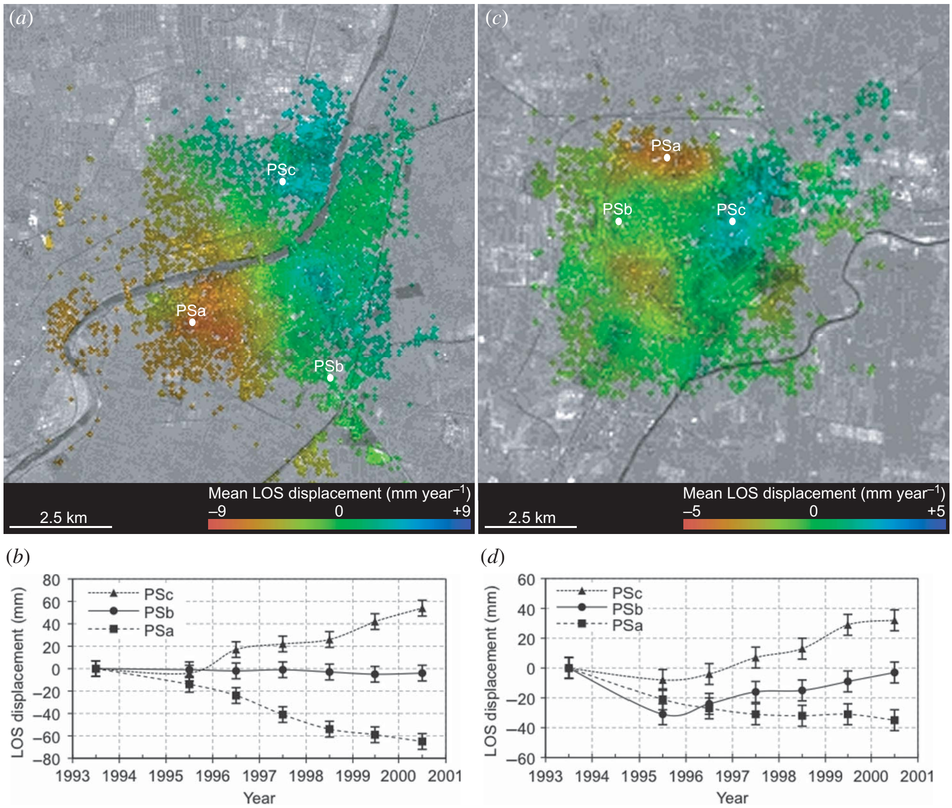

Figure 2. (*a*) Mean LOS displacements in Mansura, during 1993–2000, overlay the average amplitude image. (*b*) Deformation phase histories of PSa, PSb and PSc located in (*a*). (*c*) Mean LOS displacements in Greater Mahala during 1993–2000, superimposed on the average amplitude image. (*d*) Deformation phase histories of PSa, PSb and PSc located in (*c*).

about 65 mm of non-linear surface movement away from the satellite in the LOS direction between 1993 and 2000. The observed rate of deformation during 1998–2000 is slower than the rate of deformation between 1993 and 1998. The deformation phase history of PSb (figure 2(*b*)) shows a non-linear behaviour of deformation during 1993–2000. About 5 mm of LOS surface movement occurred away from the satellite. The deformation phase history of PSc (figure 2(*b*)) demonstrates about 4 mm of non-linear surface movement away from the satellite between 1993 and 1996 and about 54 mm towards the satellite between 1996 and 2000 (figure 2(*b*)). In Greater Mahala, the deformation phase history of PSa (figure 2(*d*)) demonstrates about 36 mm of LOS surface movement between 1993 and 2000. Nearly linear deformation occurred away from the satellite with an approximate constant rate over time from 1993 to 1998, and non-linear deformation occurred with a slower rate between 1998 and 2000. The deformation phase history of PSb (figure 2(*d*)) shows a non-linear behaviour of deformation during 1993–2000. About 31 mm of surface movement occurred during 1993–1995 and 28 mm during 1995–2000. The deformation phase history of PSc (figure 2(*d*)) demonstrates about 8 mm of non-linear surface movement away from the sensor during 1993–1997 and about 32 mm of surface movement towards the satellite during 1997–2000. It is noteworthy that the deformation rate before June 1999 is faster than the rate during the second half of 1999 and 2000 (figure 2(*c*) and 2(*d*)).

A time series of 37 LOS surface displacement maps, interpolated spatially from the initially identified PSs and referenced temporally to the earliest acquisition in the ERS data set, is created. Eight snapshots referenced to 1 July 1993, with a 1-year sampling-time interval, are then taken to show the progression of subsidence in space and time in both cities (figures 3 and 4). The measured rates of subsidence are believed to be due to groundwater processes. The bowl shapes associated with subsidence in both cities imply a major contribution from groundwater withdrawal. The aquifer system in the Nile Delta consists of alluvial sediments containing two water-bearing layers. The upper layer is a Holocene clay-silt layer of relatively low horizontal hydraulic conductivity and very low vertical permeability. The lower layer is highly permeable Pleistocene graded sand and gravel. The base of the system is the Pliocene clay (Idris and Nour 1990). The thickness of the Pleistocene aquifer is 100–900 m, with thickness decreasing towards the delta fringes and southwards to Cairo. The saturated zone of fresh water attains a maximum thickness of 300 m with less than 1000 ppm. The main recharge of the aquifer system in the delta is through infiltration from the flood irrigation and irrigation channels through the clay cap. The total annual amount of water pumped from the delta aquifer is estimated to be 1.6×10^9 m^3 (Idris and Nour 1990).

Signals of land subsidence coincide with highly populated districts in both cities. The highest rate of subsidence is observable in the southern part of Mansura and the central and northern parts of Greater Mahala (figures 3 and 4). The time series created for Greater Mahala (figure 4) shows that the subsidence bowl in the centre of the city has diminished over time, which indicates the pumping rate has been either decreased or compensated by an increased rate of water charge in the aquifer system between 1993 and 2000. Records of groundwater processes are needed for

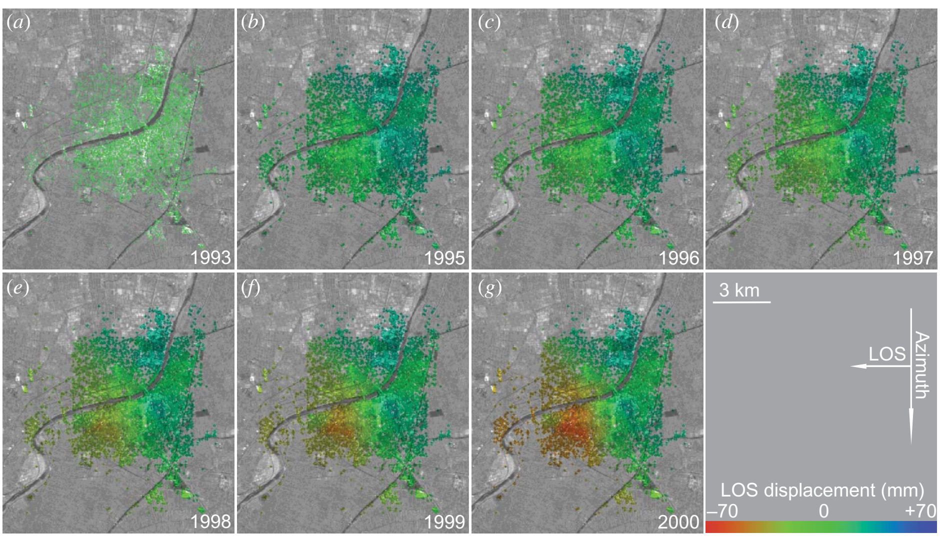

Figure 3. Estimated LOS surface displacements with 1-year sampling-time interval in Mansura from 1993 to 2000, with the average amplitude image in background. (*a*)–(*g*) are snapshots of 1 July 1993, 1995, 1996, 1997, 1998, 1999 and 2000, respectively.

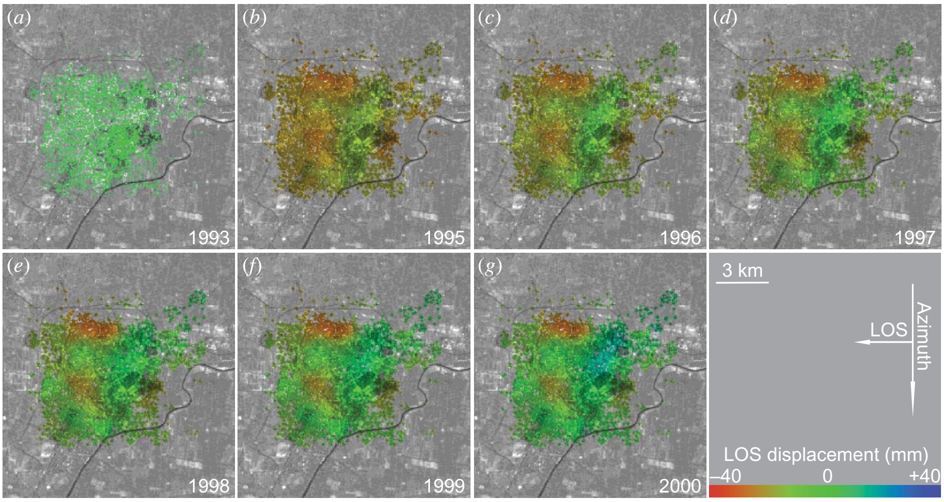

Figure 4. Estimated LOS surface displacements with 1-year sampling-time interval in Greater Mahala between 1993 and 2000. (*a*)–(*g*) are snapshots of 1 July 1993, 1995, 1996, 1997, 1998, 1999 and 2000, respectively. Displacement measurements overlay the average amplitude image.

that time period to model pumping-induced subsidence, but unfortunately historical records of groundwater charge/discharge are not available, and *in situ* measurements of subsidence have not been conducted in either city during 1993–2000. The slightly positive signals observable in the time series of surface displacements (figures 3 and 4) most likely are caused by a local system rebound resulted from local recovery of the groundwater level.

Subsidence due to the natural compaction of deltaic sediments is expected over long time periods because the stratigraphic sequence underneath the two cities contains a major fraction of clay, silt and sand. However, no regional subsidence is observed in either city during 1993–2000 (figures 3 and 4). The slight regional subsidence that may have occurred as a result of the natural sediment compaction probably has been masked by seasonal movements caused by fluctuations in the groundwater level. Also, no faults are reported underneath either Mansura or Greater Mahala; therefore, tectonic activity has no contribution to the measured rates of subsidence in both cities.

Groundwater processes may mask or amplify the signal from long-term subsidence. Consequently, more frequent InSAR data acquired over a longer time period than what we have considered in this study are needed to differentiate between the signal of pumping-induced subsidence and the signal of long-term subsidence due to the natural compaction of deltaic sediments. Such a comprehensive analysis can also help in determining areas of permanent and recoverable pumping-induced subsidence. Potential problems associated with permanent pumping-induced subsidence can be handled then by injecting water into the aquifer system, controlling the rate of groundwater pumping or eliminating pumping stations in the sites that witnessed accelerated rates of subsidence.

4. Conclusions

The Nile Delta is not an ideal environment for the application of conventional InSAR techniques because of its dense vegetation cover, high soil moisture content and high humidity. The slow rate of ground subsidence in the delta is also a major constraint because it requires a long time period to be measured, which leads to strong interferometric phase decorrelations. The cultivation process, the flood irrigation and the crop growth make the application of all InSAR techniques unfeasible over the cultivated land without using artificial reflectors. However, the PSI approach works fine over urban areas in the delta where the interferometric phase remains well correlated over considerable periods of time. PSI can overcome most of the problems associated with conventional InSAR and can precisely measure the slow rate of subsidence in the delta. But as expected, all interferograms created for Mansura and Greater Mahala are found impacted considerably by tropospheric effects due to the limited spatial extent of the urban areas in both cities that are surrounded by cultivated land. However, the interferograms created from winter acquisitions are found less affected by atmospheric artefacts than those created from summer acquisitions.

The PSI approach is capable of detecting the linear and non-linear behaviours of land subsidence in the study sites, and the time series of surface displacements shows various patterns and magnitudes of subsidence in the two cities. The major contributing factor to the measured rates of subsidence is limited to local groundwater processes in the study sites. The Nile Delta has witnessed a substantial urban development over the past century and groundwater pumping has been the primary water supply for drinking water and industrial projects. The rapid increase in the rate of groundwater pumping has resulted in a markedly increased compaction in the aquifer system.

Signals from the long-term subsidence may be masked or amplified by groundwater processes. As no regionally consistent subsidence is observed between 1993 and 2000, the slight regional subsidence expected from the natural sediment compaction most likely has been masked by surface motions caused by strong oscillations in the groundwater level. More frequent InSAR data over a longer time period than what we have considered in this investigation may help in estimating the impact of seasonal groundwater variations on the long-term subsidence due to natural sediment compaction. This can also help in determining the kinds of elastic and inelastic deformation induced by groundwater processes.

Acknowledgements

This research is supported by the Government of Egypt and the National Aeronautics and Space Administration (NASA), grant #NGT5. The raw ERS scenes are obtained from the European Space Agency (ESA) under a Category-1 proposal #2774, and the SRTM elevation data are provided by NASA-JPL. The authors are grateful to Prof. Arthur Cracknell, the editor, and two anonymous reviewers for their helpful comments and suggestions.

References

Aly, M.H., Zebker, H.A., Giardino, J.R. and Klein, A.G., 2009, Permanent scatterer investigation of land subsidence in Greater Cairo, Egypt. *Geophysical Journal International*, **178**, pp. 1238–1245.

Buckley, S., Rosen, P., Hensley, S. and Tapley, B., 2003, Land subsidence in Houston, Texas measured by radar interferometry and constrained by extensometers. *Journal of Geophysical Research*, **108**, p. 2542.

Casu, F., Buckley, S., Manzo, M., Pepe, A. and Lanari, R., 2005, Large scale InSAR deformation time series: Phoenix and Houston case studies. *IEEE International Geoscience & Remote Sensing Symposium*, **7**, pp. 5240–5243.

Dixon, T., Amelung, F., Ferretti, A., Novali, F., Rocca, F., Dokka, R., Sella, G., Kim, S., Wdowinski, S. and Whitman, D., 2006, New Orleans subsidence: space geodesy and Hurricane Katrina flooding. *Nature*, **441**, pp. 587–588.

Ferretti, A., Prati, C. and Rocca, F., 2000, Nonlinear subsidence rate estimation using permanent scatterers in differential SAR interferometry. *IEEE International Geoscience & Remote Sensing Symposium*, **38**, pp. 2202–2212.

Galloway, D., Hudnut, K., Ingebritsen, S., Phillips, S., Peltzer, G., Rogez, F. and Rosen, P., 1998, Detection of aquifer system compaction and land subsidence using interferometric synthetic aperture radar, Antelope Valley, Mojave Desert, California. *Water Resources Research*, **34**, pp. 2573–2585.

Goldstein, R. and Werner, C., 1998, Radar interferogram filtering for geophysical applications. *Geophysical Research Letters*, **25**, pp. 4035–4038.

Hoffmann, J., Zebker, H., Galloway, D. and Amelung, F., 2001, Seasonal subsidence and rebound in Las Vegas Valley, Nevada, observed by synthetic aperture radar interferometry. *Water Resources Research*, **37**, pp. 1551–1566.

Idris, H. and Nour, S., 1990, Present groundwater status in Egypt and the environmental impacts. *Environmental Geology and Water Sciences*, **16**, pp. 171–177.

Massonnet, D. and Feigl, K., 1995, Discrimination of geophysical phenomena in satellite radar interferograms. *Geophysical Research Letters*, **22**, pp. 1537–1540.

Osmanoğlu, B., Dixon, T.H., Wdowinski, S., Cabral-Cano, E. and Jiang, Y., 2011, Mexico City subsidence observed with persistent scatterer InSAR. *International Journal of Applied Earth Observation and Geoinformation*, **13**, pp. 1–12.

Scharoo, R. and Visser, P., 1998, Precise orbit determination and gravity field improvement for the ERS satellites. *Journal of Geophysical Research*, **103**, pp. 8113–8127.

Stanley, D., 1988, Subsidence in the northeastern Nile Delta: rapid rates, possible causes, and consequences. *Science*, **240**, pp. 497–500.

Stanley, D., 1990, Recent subsidence and northeast tilting of the Nile delta, Egypt. *Marine Geology*, **94**, pp. 147–154.

Stanley, D. and Warne, A., 1993, Nile Delta, recent geological evolution and human impact. *Science*, **260**, pp. 628–634.

Warne, A. and Stanley, D., 1993, Late quaternary evolution of the northwest Nile Delta and adjacent coast in the Alexandria region, Egypt. *Journal of Coastal Research*, **9**, pp. 26–64.

World Bank, 1990, *Arab Republic of Egypt: Country Economic Memorandum, Economic Readjustment with Growth*. World Bank Report No. 7447-EGT, vol. 2, 72 p. (Washington, DC: World Bank).

Zaghloul, Z., Abdel-Daiem, A. and Taha, A., 1990, Geomorphology, geologic evolution and subsidence of the Nile Delta during the Quaternary. *Bulletin of the Faculty of Science*, **17**, pp. 471–495.

Zaghloul, Z., Taha, A., Hegab, O. and El-Fawal, F., 1977, The Plio-Pleistocene Nile Delta: sub-environments, stratigraphic section and genetic classification. *Annals of the Geological Survey of Egypt*, **9**, pp. 283–291.

Zebker, H., Rosen, P. and Hensley, S., 1997, Atmospheric effects in interferometric synthetic aperture radar surface deformation and topographic maps. *Journal of Geophysical Research*, **102**, pp. 7547–7563.